THE JOURNAL OF PHYSICAL CHEMISTRY C

pubs.acs.org/JPCC Article

Rich Coverage-Dependent Carbon Phases Induced by Submonolayer Surface Segregation on Pt(111) at 78 K

X. X. Li, Q. L. Li, B. F. Miao, L. Sun, and H. F. Ding*

Cite This: J. Phys. Chem. C 2020, 124, 6716–6724 Read Online

ACCESS | Metrics & More | Article Recommendations

ABSTRACT: We report on the systematical investigation of coverage-dependent carbon phases on Pt(111) at the submonolayer (ML) regime, utilizing low energy electron diffraction and scanning tunneling microscopy. At a coverage of ~0.25 ML, carbon forms three domains with a relative rotation of 120° and each domain consists of rectangular structures, $c(4 \times 2)$-2C. When the coverage reaches ~0.3 ML, multiclusters with 7−17 atoms with an atomic arrangement of $(\sqrt{3} \times \sqrt{3})R30°$-1C are found. At ~0.5 ML, the structure changes back to a rectangular structure but with four carbon atoms in a one-unit cell, $c(4 \times 2)$-4C. At ~1.0 ML, the surface structure evolves into a close-packed (1×1) structure, that is, a three-fold structure again. Although the surface structure undergoes a series of transitions between two-fold and three-fold microscopically, the three-fold symmetry of Pt(111) is well maintained macroscopically as the rectangular structures are accompanied by three domains with a relative rotation of 120°. Our results reveal that the rich phase transitions are coverage-driven and induced by the surface segregation of carbon on Pt(111).

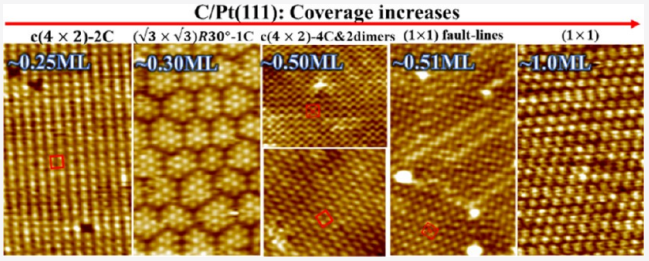

1. INTRODUCTION

Carbon has the most versatile forms in the structure, ranging from crystals of diamond, graphite, carbon nanotubes, and molecules such as fullerene to a monolayer (ML) atomic structure of graphene and graphynes.[1] Notably, the ML atomic structure of graphene has recently attracted substantial interest because of its remarkable electronic properties and strong potential for applications in electronics, composite materials, and electric batteries.[2,3] In addition to these forms, other ordered or disordered carbon overlayers on transition metals (TMs) also attract many efforts.[4−6] One of the reasons is that they may affect the activity and the selectivity of TMs as catalysts by covering the active catalyst surface and thus controlling both the rate and the product distribution of catalytic reactions.[7−9] Generally, there are two kinds of methods to introduce a carbon overlayer onto the surface of the matrix: (i) external sources by the decomposition of C-based molecules, such as carbon monoxide, methane, ethylene, benzene, and other polycyclic aromatic precursors[5,10−17] or by the direct deposition from a graphite rod[18] and (ii) internal sources by the surface segregation of carbon on carbonaceous metals.[19−24] For external sources, several ordered carbon-induced structures on TMs were explored, such as the reconstructions on the surfaces of Ni(111) and Ni(100),[15,25,26] structure with a $c(4 \times 2)$ symmetry and other more complicated structure on Re(0001),[4,6] $(\sqrt{19} \times \sqrt{19})R23.4°$, and $(\sqrt{3} \times \sqrt{3})R30°$ structures on Pt(111).[5,14] With regard to the structures of segregated carbon on platinum that we focused on in this work, some early works reported on the temperature-dependent surface carbon content and structures utilizing low energy electron diffraction (LEED) and Auger electron spectroscopy (AES).[24,27−29] For example, Lyon et al.[29] and Lambert et al.[28] annealed the Pt(111) surface at different temperatures and times and observed (2×2) and (3×3) LEED patterns of ordered carbide overlayers and ringlike LEED patterns of graphite. It is well known that one LEED pattern may correspond to different structures in real space. Thus, the detailed study on the coverage-dependent carbon structures on platinum caused by the surface segregation is still lacking.

Theoretically, the formation of carbon phases from isolated carbon atoms to graphene sheets on Pt(111) has been investigated by density functional theory (DFT).[30] The calculations show that a single carbon atom prefers to occupy a three-fold hollow face-centered (*fcc*) surface site, followed by a hexagonal-cubic-packed (*hcp*) surface site. As the content of carbon increases, the carbon atoms are predicted to aggregate in the form of C_3 trimers, dimers, and C_6 rings with the coverage of 0.33 ML, 0.5 ML, and above 0.6 ML, respectively.

Received: January 7, 2020
Revised: February 27, 2020
Published: February 28, 2020

https://dx.doi.org/10.1021/acs.jpcc.0c00160
J. Phys. Chem. C 2020, 124, 6716−6724

When the coverage of carbon is sufficiently high, a stable double layer will be formed—the first layer close-packed structure plus the upper graphene. These structures, however, still need to be experimentally confirmed.

In this work, we systematically studied the coverage-dependent carbon structures formed by surface segregation of carbon on Pt(111) utilizing LEED and scanning tunneling microscopy (STM) at 78 K. The low temperature slows down the carbon segregation process, thus facilitating the investigation of coverage-dependent phase transitions with STM. Interestingly, we observed other phases that were not predicted by DFT calculations.[30] Carbon atoms form a rectangular structure $c(4 \times 2)$-2C on top of a three-fold symmetry Pt(111) surface at a coverage of ~0.25 ML. As more carbon atoms segregate onto the surface, the surface structure successively evolves into multiclusters of a $(\sqrt{3} \times \sqrt{3})R30°$-1C structure, a rectangular $c(4 \times 2)$-4C structure, and a close-packed (1×1) structure with coverage of ~0.3 ML, ~0.5 ML, and ~1.0 ML, respectively. For the multicluster structures at ~0.3 ML, the atoms can hop between clusters but not aggregate because of the repulsion force between the atoms. This structure is different from the one predicted by the DFT calculation, which shows that carbon atoms will form C_3 species at ~0.3 ML.[30] Moreover, when the coverage reaches ~0.5 ML, dimers at some regions coexist with the $c(4 \times 2)$-4C structure. The fault lines with a (1×1) structure in the $c(4 \times 2)$-4C domain indicate the structural evolution from $c(4 \times 2)$-4C to (1×1). Microscopically, the symmetry of the structure undergoes a series of striking transitions between two-fold and three-fold with increasing carbon coverage. Macroscopically, on the contrary, the three-fold symmetry of Pt(111) is always maintained because the rectangular structures are accompanied by three domains with a relatively rotation of 120°. Our work not only enriches the knowledge of sub-ML carbon structures but also sheds light on the understanding of the catalytic properties of Pt.

2. EXPERIMENTAL SECTION

The experiments were performed in a multichamber system which is equipped with low-temperature STM, LEED, AES and a sputtering gun. The low-temperature STM is mounted in an ultrahigh vacuum (UHV) chamber with a base pressure of 2×10^{-11} mbar. LEED and AES are located in the analysis chamber (base pressure of 2×10^{-10} mbar) which connects the STM and sputtering chambers. In the sputtering chamber (base pressure of 1×10^{-9} mbar), the Pt(111) crystal (MaTeck GmbH, purity 99.99%) was prepared with cycles of Ar^+ sputtering (at 2 kV) and annealing in oxygen (870−1000 K, O_2: 1.6×10^{-7} to 5.4×10^{-5} mbar) followed by a final annealing to 1000−1300 K to remove the residual oxygen.[31] When higher partial pressure of oxygen is used, the initial carbon coverage decreased and vice versa. Accordingly, different initial carbon phases with varying coverages can be obtained by slightly changing the annealing conditions. AES measurements were made at room temperature (RT) to identify the carbon concentration at the surface. The crystal was cooled to 78 K for LEED and STM measurements. Electrochemically etched tungsten tips were used in STM measurements. The bias voltage V_s refers to the sample voltage with respect to the tip, and all the images were taken in a constant current mode. In order to avoid the influence of local defect and obtain the typical coverage-dependent STM images, we performed the measurements at many randomly pick-up scanning areas.

3. RESULTS AND DISCUSSION

We first performed the LEED measurements on the prepared sample (5 min in O_2 atmosphere with a pressure of 2.2×10^{-7} mbar at 1000 K and final anneal to 1300 K for 5 min without O_2). Figure 1a,b presents the LEED patterns obtained with

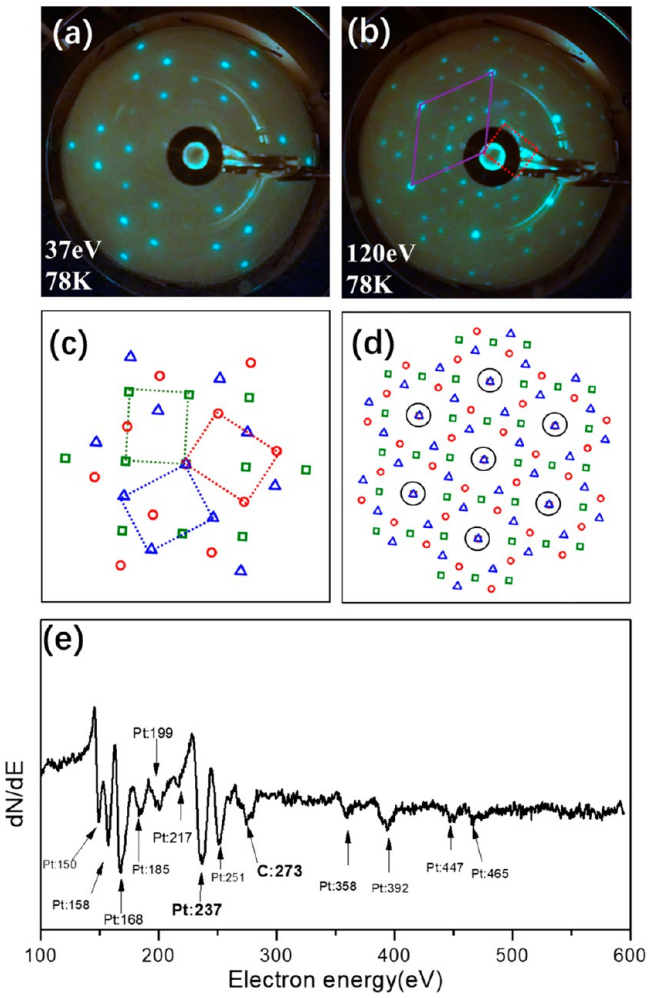

Figure 1. LEED patterns and the AES spectrum. (a,b) LEED patterns obtained at 78 K with a beam energy of 37 and 120 eV. (c,d) Schematic LEED patterns of (a,b). Green, red, and blue dotted rectangles are the three-unit cells of the surface structure. Purple solid rhombus in (b) is the unit cell of Pt(111). (e) AES spectrum of the sample.

different electron beam energies at 78 K (liquid nitrogen environment). At a beam energy of 37 eV (Figure 1a), the pattern is like a hexagram. More spots are observed as the beam energy increases to 120 eV (Figure 1b). The bright arcs observed at both the two beam energies are instrumental artefacts because they do not show any changes with the beam energy variation. Obviously, the LEED patterns show a symmetry of $c(4 \times 2)$, which has been observed on the surface of Pt(111) and Re(0001) after the adsorption of CO and the decomposition of ethylene into carbon, respectively.[3,5,32] Interestingly, in contrast to these works,[3,5,32] we did not introduce externally any carbon-based sources such as CO or ethylene molecules here. Moreover, the maximum

https://dx.doi.org/10.1021/acs.jpcc.0c00160
J. Phys. Chem. C 2020, 124, 6716−6724

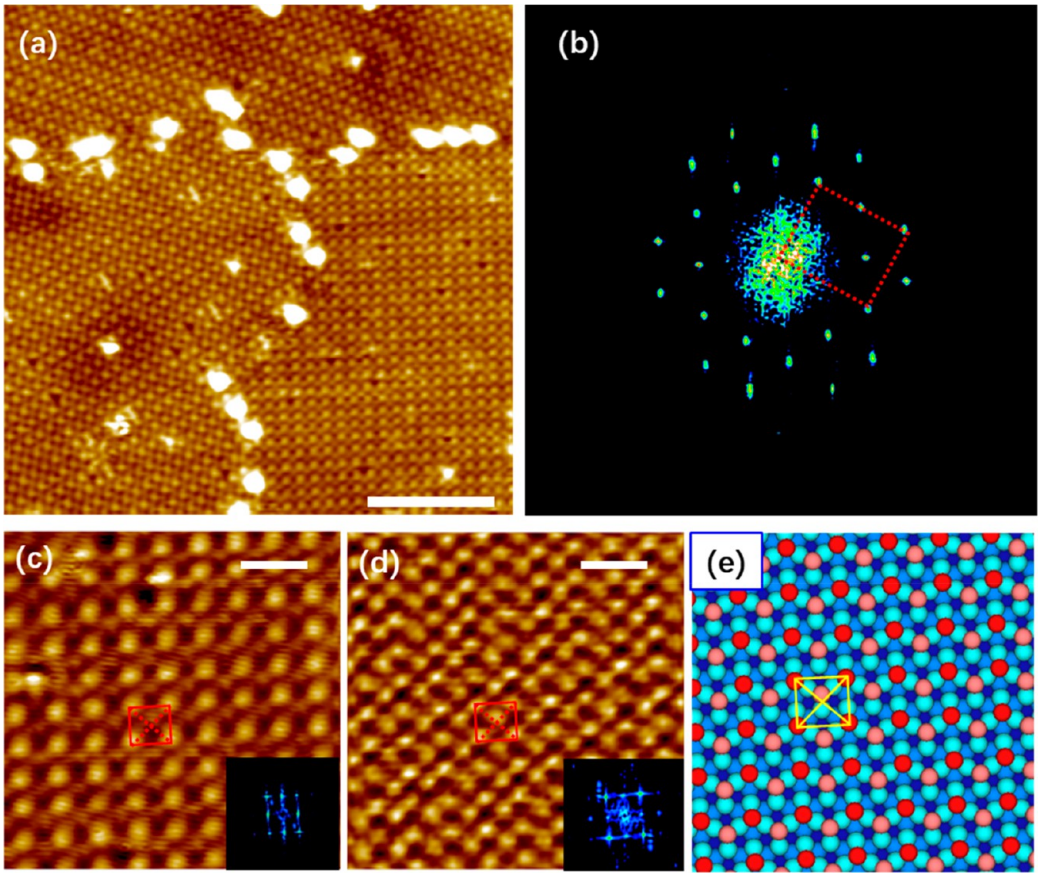

Figure 2. Typical surface topographies and the corresponding FT images obtained for ~0.5 ML carbon on Pt(111). (a) Large-scale STM image with three domains (V_s = 0.4 V, I_t = 1.0 nA, scale bar = 5 nm.). Three domains with the same structure but different orientations are separated by impurities (bright spots). (b) FT of (a). The inserted red dotted rectangle represents a one-unit cell of the rectangular structure. (c) High-resolution STM image of one domain (V_s = 0.5 V, I_t = 1.0 nA, scale bar = 1 nm). The off-center atoms are not obvious at large tunneling resistance. The inset of (c) shows the FT. (d) High-resolution STM image with a smaller tunneling resistance (V_s = 0.05 V, I_t = 1.0 nA, scale bar = 1 nm). (e) Proposed hard sphere model of $c(4 \times 2)$-4C [top first layer Pt: light blue, second layer Pt: blue, third layer Pt: deep blue, and C at different sites: red (*fcc*) and pink (*hcp*)].

increasing of the background pressure is ~1 × 10^{-9} mbar during the final annealing, and the pressure of the analysis chamber is ~2 × 10^{-10} mbar. Thus, the observed structure should originate from the segregation of impurities in the bulk Pt rather than the adsorption of external source. This will be further confirmed below by the AES spectrum and STM studies at different temperatures.

To further identify the surface elements of our sample, we characterized the sample with AES. In addition to the platinum peaks (mainly at ~237 eV), an apparent carbon peak (~273 eV)[24] can be seen in the AES spectrum (Figure 1e). There are no peaks from other elements. This is in agreement with previous studies that all impurities other than carbon could be removed by in situ sputtering and annealing.[28,31] In addition, even if a clean Pt(111) surface is obtained just after the cleaning procedure, as long as there is carbon in the bulk, a pronounced carbon signal will still be observed after a few days at RT in UHV because of the surface segregation.[31] As CO adsorbs on Pt(111) easily,[33] we also checked it with extra care. However, the signal of oxygen at ~510 eV was never observed, which is strongly contrasted to previous reports on Pt(111) with CO adsorption.[34−36] Hitherto, we can conclude that the LEED patterns result from the surface segregation of carbon. Note that the energy valley of carbon locates at ~273 eV, very close to that of graphite obtained in the previous AES measurement.[37] However, the typical ratio between the carbon peak (~273 eV) and the platinum peak (~237 eV) is ~0.3, which is much less than the values of ~0.8, ~0.6, and 3.8 for carbide, graphite islands, and the graphite layer, respectively,[28,38,39] suggesting that the rather low concentration of carbon obtained here is not sufficient to form carbide or graphite layers, as reported previously. This is consistent with the LEED pattern of the hexagram-like diffraction spots with $c(4 \times 2)$ symmetry (Figure 1a) rather than (2×2), (3×3) or typical ring-like diffraction spots of graphene on Pt(111), as in previous studies.[28,29,40−43] Although we cannot completely rule out the existence of other extremely small amounts of impurities which has a significant influence on the surface structure because of the sensitivity limitation of AES, our STM studies (to be discussed below) did not find any other apparent impurities; thus, the influence of other impurities is unlikely.

Through the comparison with the STM images which will be discussed below, the diffraction pattern can be interpreted as a superposition of three rotational domains with an angle of 120° with each other, which are represented by red circles, green rectangles, and blue triangles in Figure 1c,d, respectively. The corresponding unit cells are marked in Figure 1c. Note that the diffraction spots of these three domains overlap at the

https://dx.doi.org/10.1021/acs.jpcc.0c00160
J. Phys. Chem. C 2020, 124, 6716−6724

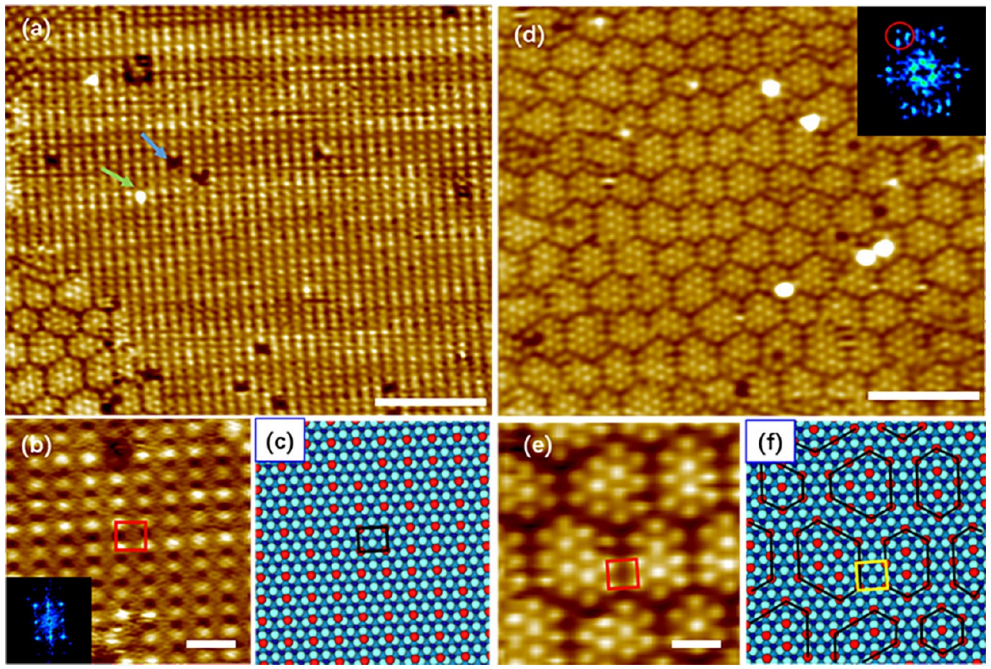

Figure 3. $c(4 \times 2)$-2C and multiclusters of $(\sqrt{3} \times \sqrt{3})R30°$-1C structures. (a) Coexistence of $c(4 \times 2)$-2C and multiclusters of the $(\sqrt{3} \times \sqrt{3})R30°$-1C structure at $\theta_C \approx 0.255$ ML. Blue and green arrows mark the carbon vacancy and the impurity, respectively. (V_s = 0.5 V, I_t = 1.0 nA, scale bar = 5 nm). (b) High-resolution STM image of the $c(4 \times 2)$-2C structure. (V_s = 0.05 V, I_t = 1.0 nA, scale bar = 1 nm). (c) Proposed hard sphere model of the $c(4 \times 2)$-2C structure in (b). (d) Multiclusters of the $(\sqrt{3} \times \sqrt{3})R30°$-1C structure with $\theta_C \approx 0.302$ ML (V_s = 0.5 V, I_t = 1.0 nA, scale bar = 5 nm). (e) High-resolution image of multiclusters of $(\sqrt{3} \times \sqrt{3})R30°$-1C structure ($V_s$ = 0.5 V, I_t = 1.0 nA, scale bar = 1 nm). (f) Proposed hard sphere model of (e) (first layer Pt: light blue, second layer Pt: blue, third layer Pt: deep blue, and C: red).

positions of the spots from Pt(111) (larger black circles in Figure 1d).

In order to obtain the specific surface structure of these carbon atoms in real space, the sample was cooled to 78 K within ~40 min after the cleaning procedure, and the STM images were obtained at multiple locations across the sample. The STM image in Figure 2a presents three domains oriented at 120° to each other with a few large and bright impurities on the boundaries of the domains. The tunneling condition is V_s = 0.4 V and I_t = 1.0 nA. Figure 2b is the Fourier transform (FT) image of these three domains. As shown in the high resolution of one domain in Figure 2c, the width and length of the rectangle is about $\sqrt{3}a$ and $2a$, respectively [$a \approx 2.78$ Å is the nearest distance between platinum atoms on the Pt(111) surface]. Note, the other two domains have the same atomic structure but with an angle of 120° in-plane rotation to each other. The corresponding FT image of this domain is inserted at the bottom right of Figure 2c. Obviously, the FT image in Figure 2b is a combination of the three FT images of these three domains, in good agreement with the LEED pattern shown in Figure 1a. Now, it is clear that the obtained LEED pattern corresponds to the real-space rectangular structure of three domains with a relative rotation of 120°. For the sake of clarity, only one rectangular cell is marked by a red dotted rectangle in Figure 2b.

Note that this rectangular structure is similar to the structure of CO adsorption on Pt(111).[33] However, the detailed structures are actually different. In the rectangular structure, the C atom is off-centered in our structure (Figure 2c,d at different bias), while the CO molecular is reported to be located exactly at the center of the rectangle. The site of the off-center atom is illustrated by the rectangle with crossing diagonals in Figure 2c. This can be viewed better with the scanning condition of a lower tunneling resistance (V_s = 0.05 V, I_t = 1.0 nA), as shown in Figure 2d. It shows that the off-center atom has almost the same size with the corner atoms (Figure 2d), while it is a small spot in Figure 2c. Similarly, the bias-dependent morphology of the off-center atom also exists in the other two domains. We speculate that the corner and off-center atoms occupy different hollow sites. In fact, previous calculations have shown that carbon atoms prefer to occupy either three-fold hollow *fcc* or *hcp* surface sites on Pt(111) with slightly different heights. The proposed atomic model is shown in Figure 2e. The corner and off-center atoms occupy different sites. We name this structure as $c(4 \times 2)$-4C by conventional notation of ordered adsorption on a crystal surface.[44] The carbon coverage θ_C is defined by the ratio of the density of the surface carbon atoms to the density of the platinum atoms at the surface. Thus, the carbon coverage of the $c(4 \times 2)$-4C structure is 0.5 ML.

It is well practiced that the surface carbon atoms can be removed by oxidation in a high temperature oxygen atmosphere.[31,45] Through multiple trials, we found that the initial coverage of carbon obtained by STM at 78 K depends on the oxygen content, temperature, time during the annealing process, and the rate of cooling. If the oxygen content increases, the initial coverage decreases. We increased the oxygen concentration and decreased the final annealing temperature from 1300 to 1000 K during the annealing process to reduce the surface carbon atoms further (5 min in O_2: 5.4×10^{-5} mbar at 1000 K and final anneal at 1000 K for 5 min without O_2). Then, a coexistence of rectangular lattices and a small number of hexagonal lattices were obtained (Figure 3a). From a large-scale image in Figure 3a, this

https://dx.doi.org/10.1021/acs.jpcc.0c00160
J. Phys. Chem. C 2020, 124, 6716−6724

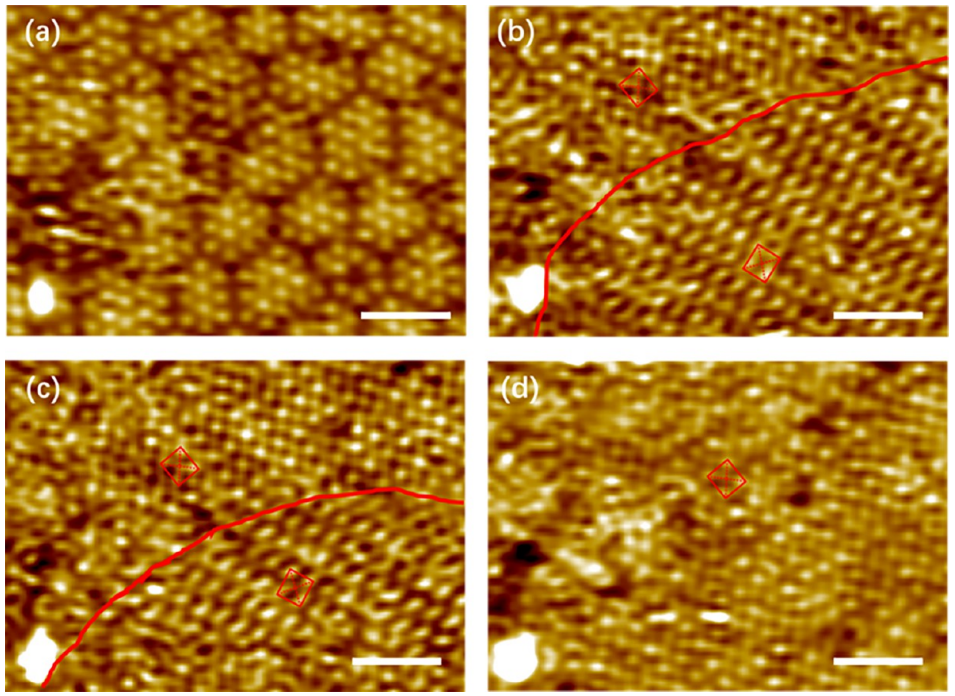

Figure 4. Phase transition from multiclusters of $(\sqrt{3} \times \sqrt{3})R30°$-1C to $c(4 \times 2)$-4C structures at 78 K. (a) Multiclusters of the $(\sqrt{3} \times \sqrt{3})R30°$-1C structure. (b) 12 min after (a), the $(\sqrt{3} \times \sqrt{3})R30°$-1C structure changes to the $c(4 \times 2)$-4C structure with two domains separated by a red curve. (c) 8 min after (b), the domain at the top left expands. (d) 3 min after (c), the whole area is occupied by one domain. V_s = 0.5 V, I_t = 1.0 nA, scale bar = 2 nm.

rectangular structure is nearly identical to the $c(4 \times 2)$-4C structure discussed above except that there are fewer impurities (green arrow) and more vacancies (blue arrow). The zoomed-in high resolution image (Figure 3b), however, shows that the structure is different as there is no carbon atom within the rectangle. Thus, this structure is $c(4 \times 2)$-2C and it appears at the coverage of 0.25 ML. As shown in proposed atomic model in Figure 3c, all carbon atoms occupy the same *fcc* sites located at the corner position of the rectangle.

In the lower left corner of Figure 3a, there are small amounts of irregular polygonal structures composed of 7−17 carbon atoms. The arrangement of the atoms within these multicluster structures is $(\sqrt{3} \times \sqrt{3})R30°$-1C. The coverage of carbon atoms of this structure is ∼0.3 ML, which is slightly greater than the coverage of $c(4 \times 2)$-2C. Nevertheless, the relative area of the $(\sqrt{3} \times \sqrt{3})R30°$-1C structure with respect to the entire area is very small. It is about 10% because the overall coverage of the entire area (Figure 3a) is ∼0.255 ML, very close to the ideal coverage for the $c(4 \times 2)$-2C structure. It is worth mentioning that this structure is not very stable at 78 K as the surface segregation of carbon leads to the expansion of the area of multiclusters of the $(\sqrt{3} \times \sqrt{3})R30°$-1C structure and the shrinking area of the $c(4 \times 2)$-2C structure. The surface segregation behavior of carbon at a low temperature 78 K can be explained by the DFT calculation reported by Janthon et al.[46] When the subsurface sites are taken into consideration, calculated results reveal that the tetrahedral subsurface (*tss*) sites are almost isoenergetic to surface *fcc* and *hcp* sites. In addition, the low energy barrier between surface *hcp* sites and subsurface *tss* provides the possibility for carbon atoms to segregate from bulk at low temperature. It is emphasized that the surface segregation is rather slow at 78 K.

Besides the surface segregation of carbon atoms at 78 K, which can lead to the expanding area of the $(\sqrt{3} \times \sqrt{3})R30°$-1C structure, the initial multiclusters of the $(\sqrt{3} \times \sqrt{3})R30°$-1C structure (Figure 3d) that almost completely covered the surface can also be obtained by decreasing the oxygen concentration and increasing the final annealing temperature from 1000 to 1200 K during the annealing process. As shown in the high-resolution STM image Figure 3e and the corresponding proposed model Figure 3f, the edge atoms of two adjacent clusters form a $c(4 \times 2)$-2C structure, as marked by the rectangles in Figure 3e,f. It is interesting to note that the clusters in Figure 3d also form a self-organized close-packed pattern with a period of ∼2 nm as also visible in the inserted FT, where the diffraction spot of the $(\sqrt{3} \times \sqrt{3})R30°$-1C structure splits to three spots, as marked by the red circle. Surprisingly, we noticed that the number of atoms within the individual clusters and the shape of the clusters were not always fixed. By comparing images obtained from multiple scans at the same region, we found that the atoms at the edge of one cluster could jump to the edge of its neighboring cluster occasionally at 78 K. Previous calculations have estimated that the optimum diffusion temperature of a single carbon atom between the *fcc* and *hcp* sites was 475 ± 10 K.[30] However, the diffusion rate is not zero at lower temperatures. Thus, the diffusion is possible but with a reduced probability.

The low temperature of 78 K slows down the rate of surface segregation of carbon, allowing the detailed investigation of the transition between different phases. A typical phase transition process is shown in Figure 4. After multiple scans (∼12 min in total) at the same region, multiclusters of the $(\sqrt{3} \times \sqrt{3})R30°$-1C structure evolve into the $c(4 \times 2)$-4C structure. In the initial stage of transition, two domains with

https://dx.doi.org/10.1021/acs.jpcc.0c00160
J. Phys. Chem. C 2020, 124, 6716−6724

the $c(4 \times 2)$-4C structure appear, as shown in Figure 4b. After about 8 min, the area of the domain in the upper left corner expands (Figure 4c). Three minutes after taking the image of Figure 4c, it occupies the entire surface, as shown in Figure 4d. As a result, the carbon coverage changes from ∼0.3 ML to ∼0.5 ML. Because of the movements of the carbon atoms, the morphology during the transition is not very clear. When the sample was placed at 78 K for more than 12 h, the system tended to be thermodynamically equilibrium. A clearer $c(4 \times 2)$-4C structure could be obtained. At the same time, many large impurities appeared at the boundaries of the domains.

In addition to the monomer atomic structure, we also observed a dimer structure in some localized regions at a coverage of ∼0.5 ML. As shown in Figure 5a, the rectangular

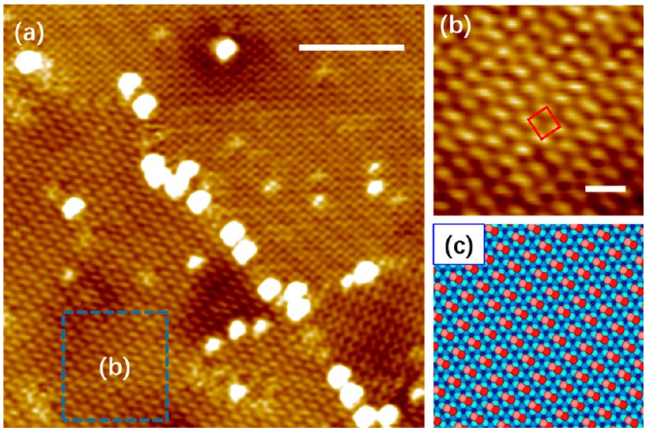

Figure 5. $c(4 \times 2)$-4C monomer atomic and $c(4 \times 2)$-2dimers structures at ∼0.5 ML. (a) Coexistence of $c(4 \times 2)$-2dimers and $c(4 \times 2)$-4C monomer atomic structures (V_s = 0.05 V, I_t = 1.0 nA, scale bar = 5 nm). (b) Zoomed-in STM image of the marked region in (a) (V_s = 0.05 V, I_t = 1.0 nA, scale bar = 1 nm). (c) Hard sphere model of the $c(4 \times 2)$-2dimers in (b) [first layer Pt: light blue, second layer Pt: blue, third layer Pt: deep blue, and C at different sites: red (*fcc*) and pink (*hcp*)].

structure composed of dimers coexists with the $c(4 \times 2)$-4C structure, and many large impurities appear at the boundaries of the domains. The zoomed-in image of the dimer structure is shown in Figure 5b. Within the dimer structure, the calculation indicates that two carbon atoms are separated by 137 pm, one occupying the *fcc* site and the other one occupying the neighboring *hcp* site.[30] The distance between these two atoms is so small that the dimers appear larger and longer than the individual atoms in the STM image. We find that the rectangle composed by dimers also has the same size of the unit cell of the monomer structure. Thus, we name it as the $c(4 \times 2)$-2dimers structure. According to the DFT calculations, dimers are more stable than two single atoms when the surface carbon coverage reaches 0.5 ML.[30] The experimental statistics, however, shows that the monomer structure appears more often than the dimer structure. Nevertheless, the coexisting of both structures suggests that the energy difference between these two structures is small. To illustrate the dimer structure better, we also construct a specific atomic model, as shown in Figure 5c.

In order to investigate the structural transition from 0.5 ML to a higher coverage caused by the surface segregation of carbon atoms, we kept the sample at 78 K in the UHV chamber for more than 3 weeks and performed STM measurements every few days. As time went on, we found that except for some increasing fault lines and impurities at scattered areas (Figure 6a), most of the regions still maintain the $c(4 \times 2)$-4C structure, which indicates the rate of carbon segregation is greatly reduced and the system is gradually approaching its equilibrium state. The arrangement of atoms within the fault lines is (1×1), and the proposed atomic model of this structure is shown in Figure 6b with a coverage of ∼0.55 ML. Moreover, the density of fault lines and bright impurities increased slowly with time. We therefore speculate that the fault line is a building block of the close-packed (1×1) structure. If the density of the fault lines is sufficiently high, they will eventually form a (1×1) structure over the entire surface and the corresponding surface coverage will reach 1.0 ML. It is worth mentioning that the phase transition from $c(4 \times 2)$-4C to (1×1) is much slower than that from $(\sqrt{3} \times \sqrt{3})R30°$-1C to $c(4 \times 2)$-4C, that is, the coverage from ∼0.5 ML to ∼1.0 ML is much slower than that from ∼0.3 ML to ∼0.5 ML.

As demonstrated above, the rate of carbon segregation at 78 K slows down after the coverage reaches ∼0.5 ML, so it will take a very long time for $c(4 \times 2)$-4C to completely evolve to the (1×1) structure. Alternatively, annealing the substrate in lower or even no oxygen for 30 min (1000 K, 30 min), we also obtain the almost fully-coverage (1×1) structure (Figure 6c). In this structure, all carbon atoms occupy same sites, as shown in the proposed hard sphere model in Figure 6d. Note that after prolonged annealing (15 min at ∼1300 K without oxygen), more carbon segregated from bulk to the surface, and then, we did observe graphene nanosheets with sizes of ∼10 nm with moiré patterns at some regions in STM images, as has been reported.[16,39,43,47−50] This is consistent with the double-layer model, which consists of a close-packed carbon structure and a graphene layer.[30,51] Thus, our results are not in conflict with previous studies.

As discussed above, there are some similarities between the structures induced by surface segregation of carbon and the adsorption of CO.[33] To further exclude that our observation is caused by the adsorption of CO, we performed control experiments at different temperatures. It is generally accepted that gas adsorption is stronger at lower temperature,[44,52] while surface segregation will slow down when the temperature is reduced. Thus, for the samples prepared with the same conditions but preserved at different temperatures, the coverage would be different. When the effect is dominant by the gas adsorption, the observed coverage would be higher at lower temperatures. On the contrary, when it is caused by the surface segregation, the coverage would be lower at lower temperatures. Figure 7 presents the STM images of the sample prepared under almost the same conditions but preserved at 4.7 K (liquid He) (a), 78 K (liquid nitrogen) (b), and 300 K (RT) (c). All the images are taken ∼40 min after transferring the sample to the STM stage. It shows that the coverage is ∼0.3 ML at 4.7 K, ∼0.5 ML at 78 K, and ∼1 ML at 300 K, which indicates that the observed phenomenon is dominated by surface segregation. Moreover, a high coverage adsorption of CO is difficult in a UHV chamber and the maximum coverage of CO adsorption is only ∼0.56 ML, as reported by Yang et al., upon CO dosing at ∼50 K,[33] which is in sharp contrast to the coverage (∼1 ML) that we observed at 300 K. In addition, if the observed effect is caused by the CO adsorption, one would expect to observe an O-peak at 510 eV, as reported previously.[34−36] This is, however, not observed

https://dx.doi.org/10.1021/acs.jpcc.0c00160
J. Phys. Chem. C 2020, 124, 6716−6724

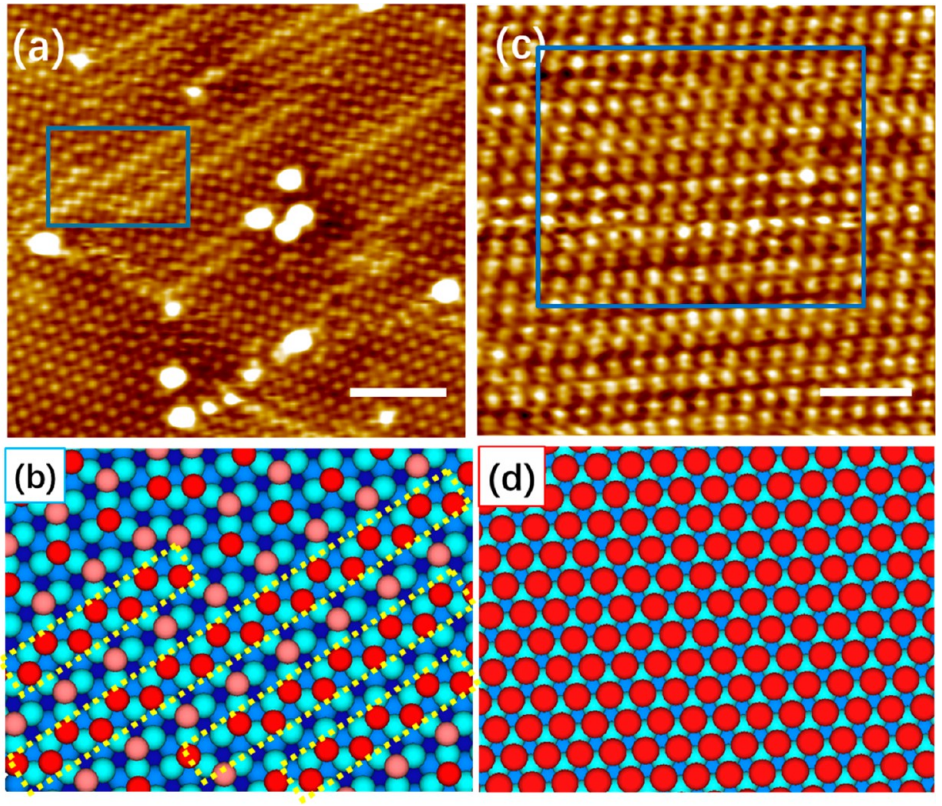

Figure 6. Fault lines in $c(4 \times 2)$-4C domain and (1×1) structure. (a) After several weeks at 78 K, some large impurities and fault lines with the (1×1) structure appear among the $c(4 \times 2)$-4C structure (V_s = 0.2 V, I_t = 1.0 nA, scale bar = 3 nm). (b) Proposed hard sphere model of the structure in the rectangle in (a) with a coverage of ~0.548 ML. (c) (1×1) structure after longer time of annealing (V_s = 0.5 V, I_t = 1.0 nA, scale bar = 1 nm). (d) Proposed hard sphere model of the (1×1) structure in the rectangle area in (c) [top first layer Pt: light blue, second layer Pt: blue, third layer Pt: deep blue, and C at different sites: red (*fcc*) and pink (*hcp*)].

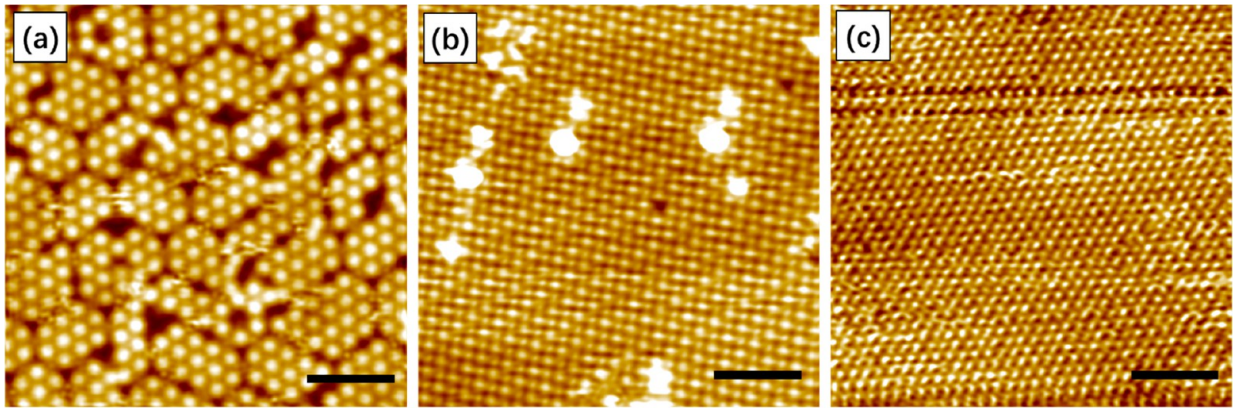

Figure 7. Same prepared sample measured at 4.7 K (liquid He), 78 K (liquid nitrogen), and 300 K (RT). (a) $(\sqrt{3} \times \sqrt{3})R30°$-1C at 4.7 K with $\theta_C \approx 0.3$ ML (V_s = 0.1 V, I_t = 1.0 nA, scale bar = 2 nm). (b) $c(4 \times 2)$-4C structure at 78 K with $\theta_C \approx 0.5$ ML (V_s = 0.1 V, I_t = 1.0 nA, scale bar = 2 nm). (c) (1×1) structure at 300 K with $\theta_C \approx 1.0$ ML (V_s = 0.2 V, I_t = 1.0 nA, scale bar = 2 nm).

(Figure 1e) in our case, as we discussed above. Thus, we can exclude that the effect is caused by CO adsorption and conclude that it is indeed due to the C-segregation from the bulk.

4. CONCLUSIONS

In conclusion, we observed rich coverage-dependent carbon structures because of the slow surface segregation of carbon on Pt(111) at 78 K utilizing STM. The coverage-dependent structures and corresponding lattice descriptions are summarized in Table 1. At a coverage of ~0.25 ML, carbon atoms form three domains with 120° rotation to each other and each of the domain consists of a two-fold symmetry structure $c(4 \times 2)$-2C. As the carbon coverage increases because of surface segregation, phase transition happens. The carbon phase evolves to multicluster structures at a coverage of ~0.3 ML. The arrangement of the atoms within clusters is $(\sqrt{3} \times \sqrt{3})R30°$-1C, and 7−17 carbon atoms compose each of the cluster. The carbon atoms can hop between neighboring clusters occasionally but not aggregate because of

https://dx.doi.org/10.1021/acs.jpcc.0c00160
J. Phys. Chem. C 2020, 124, 6716−6724

Table 1. Summary of Coverage-Dependent Carbon Structures on Pt(111) and Corresponding Lattice Descriptions

coverage (ML)	structure	description
~0.25	$c(4 \times 2)$-2C	rectangle (3 domains)
~0.30	multi-clusters $(\sqrt{3} \times \sqrt{3})R30°$-1C	triangle
~0.50	$c(4 \times 2)$-4C $c(4 \times 2)$-2dimers	rectangle with an off-center atom rectangle (3 domains)
~0.55	(1×1) fault lines in $c(4 \times 2)$-4C domain	rectangle (3 domains)
~1.00	(1×1) close-packed	triangle

the repulsion between atoms. With further increasing coverage to ~0.5 ML, the structure changes back to a rectangular structure but with the $c(4 \times 2)$-4C structure, and carbon dimers are also observed at some regions. Finally, the structure evolves to a three-fold close-packed (1×1) structure with a coverage of ~1.0 ML. Even though there are rectangular structures microscopically at coverages of ~0.25 ML and ~0.5 ML, the three-fold symmetry of Pt(111) is still maintained macroscopically as rectangular structures are accompanied by three domains with a relative rotation of 120°. Our research extends knowledge into the coverage-dependent carbon structure evolution on Pt(111). Note that recent simulations show that subsurface C species are able to form even in a coinage noble-metal system.[53] Moreover, a similar experiment on the influence of subsurface oxygen on the properties of Pd(111) has also been studied.[54] For platinum, the experimental identification of subsurface C and the mechanism of its influence on catalytic properties will be an interesting work to explore in future.

AUTHOR INFORMATION

Corresponding Author

H. F. Ding − *National Laboratory of Solid State Microstructures and Department of Physics and Collaborative Innovation Center of Advanced Microstructures, Nanjing University, Nanjing 210093, China;* orcid.org/0000-0001-7524-0779; Email: hfding@nju.edu.cn

Authors

X. X. Li − *National Laboratory of Solid State Microstructures and Department of Physics, Nanjing University, Nanjing 210093, China*

Q. L. Li − *National Laboratory of Solid State Microstructures and Department of Physics, Nanjing University, Nanjing 210093, China*

B. F. Miao − *National Laboratory of Solid State Microstructures and Department of Physics and Collaborative Innovation Center of Advanced Microstructures, Nanjing University, Nanjing 210093, China*

L. Sun − *National Laboratory of Solid State Microstructures and Department of Physics and Collaborative Innovation Center of Advanced Microstructures, Nanjing University, Nanjing 210093, China*

Complete contact information is available at: https://pubs.acs.org/10.1021/acs.jpcc.0c00160

Notes

The authors declare no competing financial interest.

ACKNOWLEDGMENTS

This work was supported by the National Key R&D Program of China (grants no. 2017YFA0303202, and no. 2018YFA0306004); the National Natural Science Foundation of China (grants no. 11974165, no. 51971110, and no. 11734006); the China Postdoctoral Science Foundation (grant no. 2019M651766); and the Natural Science Foundation of Jiangsu Province (grant no. BK20190057).

REFERENCES

(1) Malko, D.; Neiss, C.; Viñes, F.; Görling, A. Competition for Graphene: Graphynes with Direction-Dependent Dirac Cones. *Phys. Rev. Lett.* **2012**, *108*, 086804.

(2) Geim, A. K.; Novoselov, K. S. The Rise of Graphene. *Nat. Mater.* **2007**, *6*, 183−191.

(3) Zhang, Y.; Tan, Y.-W.; Stormer, H. L.; Kim, P. Experimental Observation of the Quantum Hall Effect and Berry's Phase in Graphene. *Nature* **2005**, *438*, 201−204.

(4) Miniussi, E.; Pozzo, M.; Menteş, T. O.; Niño, M. A.; Locatelli, A.; Vesselli, E.; Comelli, G.; Lizzit, S.; Alfè, D.; Baraldi, A. The Competition for Graphene Formation on Re(0001): A Complex Interplay between Carbon Segregation, Dissolution and Carburisation. *Carbon* **2014**, *73*, 389−402.

(5) Fujita, T.; Kobayashi, W.; Oshima, C. Novel Structures of Carbon Layers on a Pt(111) Surface. *Surf. Interface Anal.* **2005**, *37*, 120−123.

(6) Ducros, R.; Housley, M.; Alnot, M.; Cassuto, A. Ethylene and Acetylene Adsorption on Rhenium Polycrystalline and Re(0001) Surfaces. *Surf. Sci.* **1978**, *71*, 433−446.

(7) Argyle, M.; Bartholomew, C. Heterogeneous Catalyst Deactivation and Regeneration: A Review. *Catalysts* **2015**, *5*, 145−269.

(8) Borodziński, A.; Bond, G. C. Selective Hydrogenation of Ethyne in Ethene-Rich Streams on Palladium Catalysts. Part 1. Effect of Changes to the Catalyst During Reaction. *Catal. Rev.* **2006**, *48*, 91−144.

(9) Blakely, D. W.; Somorjai, G. A. The Dehydrogenation and Hydrogenolysis of Cyclohexane and Cyclohexene on Stepped (High Miller Index) Platinum Surfaces. *J. Catal.* **1976**, *42*, 181−196.

(10) Nam, J.; Kim, D.-C.; Yun, H.; Shin, D. H.; Nam, S.; Lee, W. K.; Hwang, J. Y.; Lee, S. W.; Weman, H.; Kim, K. S. Chemical Vapor Deposition of Graphene on Platinum: Growth and Substrate Interaction. *Carbon* **2017**, *111*, 733−740.

(11) Kim, H. W.; Ku, J.; Ko, W.; Cho, Y.; Jeon, I.; Hwang, S. W. Quenching of the Resonant States of Single Carbon Vacancies in Graphene/Pt(111). *J. Phys. Chem. C* **2017**, *121*, 24641−24647.

(12) Feng, X.; Wu, J.; Bell, A. T.; Salmeron, M. An Atomic-Scale View of the Nucleation and Growth of Graphene Islands on Pt Surfaces. *J. Phys. Chem. C* **2015**, *119*, 7124−7129.

(13) Sun, J.; Nam, Y.; Lindvall, N.; Cole, M. T.; Teo, K. B. K.; Woo Park, Y.; Yurgens, A. Growth Mechanism of Graphene on Platinum: Surface Catalysis and Carbon Segregation. *Appl. Phys. Lett.* **2014**, *104*, 152107.

(14) Otero, G.; González, C.; Pinardi, A. L.; Merino, P.; Gardonio, S.; Lizzit, S.; Blanco-Rey, M.; Van de Ruit, K.; Flipse, C. F. J.; Méndez, J.; de Andrés, P. L.; Martín-Gago, J. A. Ordered Vacancy Network Induced by the Growth of Epitaxial Graphene on Pt(111). *Phys. Rev. Lett.* **2010**, *105*, 216102.

(15) Nakano, H.; Nakamura, J. Carbide-Induced Reconstruction Initiated at Step Edges on Ni(111). *Surf. Sci.* **2001**, *482−485*, 341−345.

(16) Land, T. A.; Michely, T.; Behm, R. J.; Hemminger, J. C.; Comsa, G. Direct Observation of Surface Reactions by Scanning Tunneling Microscopy: Ethylene→Ethylidyne→Carbon Particles→Graphite on Pt(111). *J. Chem. Phys.* **1992**, *97*, 6774−6783.

(17) Levy, N.; Burke, S. A.; Meaker, K. L.; Panlasigui, M.; Zettl, A.; Guinea, F.; Neto, A. H. C.; Crommie, M. F. Strain-Induced Pseudo-

https://dx.doi.org/10.1021/acs.jpcc.0c00160
J. Phys. Chem. C 2020, 124, 6716−6724

Magnetic Fields Greater Than 300 Tesla in Graphene Nanobubbles. *Science* **2010**, *329*, 544−547.
(18) Loginova, E.; Nie, S.; Thürmer, K.; Bartelt, N. C.; McCarty, K. F. Defects of Graphene on Ir(111): Rotational Domains and Ridges. *Phys. Rev. B* **2009**, *80*, 085430.
(19) Gao, J.-H.; Sagisaka, K.; Kitahara, M.; Xu, M.-S.; Miyamoto, S.; Fujita, D. Graphene Growth on a Pt(111) Substrate by Surface Segregation and Precipitation. *Nanotechnology* **2012**, *23*, 055704.
(20) Marchini, S.; Günther, S.; Wintterlin, J. Scanning Tunneling Microscopy of Graphene on Ru(0001). *Phys. Rev. B* **2007**, *76*, 075429.
(21) Fujita, D.; Schleberger, M.; Tougaard, S. XPS Study of the Surface Enrichment Process of Carbon on C-Doped Ni(111) Using Inelastic Background Analysis. *Surf. Sci.* **1995**, *331*−*333*, 343−348.
(22) Fujita, D.; Yoshihara, K. Surface Precipitation Process of Epitaxially Grown Graphite (0001) Layers on Carbon-Doped Nickel(111) Surface. *J. Vac. Sci. Technol. A* **1994**, *12*, 2134−2139.
(23) Yamazaki, S.; Tanaka, M.; Tanaka, S.; Fuginami, M.; Uemori, R.; Fujita, D.; Homma, T.; Ono, M. Atomic Images and Defect Structures of the Epitaxially Precipitated Carbon Layers on Ni(111) Surface. *J. Vac. Sci. Technol. B* **1991**, *9*, 883−885.
(24) Hamilton, J. C.; Blakely, J. M. Carbon Layer Formation on Pt (111) Surface as a Function of Temperature. *J. Vac. Sci. Technol.* **1978**, *15*, 559−562.
(25) Klink, C.; Stensgaard, I.; Besenbacher, F.; Lægsgaard, E. An STM Study of Carbon-Induced Structures on Ni(111): Evidence for a Carbidic-Phase Clock Reconstruction. *Surf. Sci.* **1995**, *342*, 250−260.
(26) Klink, C.; Olesen, L.; Besenbacher, F.; Stensgaard, I.; Laegsgaard, E.; Lang, N. D. Interaction of C with Ni(100): Atom-Resolved Studies of the "Clock" Reconstruction. *Phys. Rev. Lett.* **1993**, *71*, 4350−4353.
(27) Hamilton, J. C.; Blakely, J. M. Carbon Segregation to Single Crystal Surfaces of Pt, Pd and Co. *Surf. Sci.* **1980**, *91*, 199−217.
(28) Lambert, R. M.; Weinberg, W. H.; Comrie, C. M.; Linnett, J. W. LEED-Auger Investigation of a Stable Carbide Overlayer on a Platinum (111) Surface. *Surf. Sci.* **1971**, *27*, 653−658.
(29) Lyon, H. B.; Somorjai, G. A. Low-Energy Electron-Diffraction Study of Clean (100), (111), and (110) Faces of Platinum. *J. Chem. Phys.* **1967**, *46*, 2539−2550.
(30) Viñes, F.; Neyman, K. M.; Görling, A. Carbon on Platinum Substrates: From Carbidic to Graphitic Phases on the (111) Surface and on Nanoparticles. *J. Phys. Chem. A* **2009**, *113*, 11963−11973.
(31) Wrobel, R. J.; Becker, S. Carbon and Sulphur on Pd(111) and Pt(111): Experimental Problems During Cleaning of the Substrates and Impact of Sulphur on the Redox Properties of CeOx in the CeOx/Pd(111) System. *Vacuum* **2010**, *84*, 1258−1265.
(32) Tüshaus, M.; Schweizer, E.; Hollins, P.; Bradshaw, A. M. Yet Another Vibrational Study of the Adsorption System Pt{111}-CO. *J. Electron Spectrosc. Relat. Phenom.* **1987**, *44*, 305−316.
(33) Yang, H. J.; Minato, T.; Kawai, M.; Kim, Y. STM Investigation of CO Ordering on Pt(111): From an Isolated Molecule to High-Coverage Superstructures. *J. Phys. Chem. C* **2013**, *117*, 16429−16437.
(34) Lin, W. F.; Zei, M. S.; Ertl, G. Identification of the Structure of a CO Adlayer on a Pt(111) Electrode. *Chem. Phys. Lett.* **1999**, *312*, 1−6.
(35) Rhee, C. K.; Feliu, J. M.; Herrero, E.; Mrozek, P.; Wieckowski, A. Auger Electron Spectroscopy, Low-Energy Electron Diffraction, and Electrochemistry of Carbon Monoxide on a Pt(100) Electrode. *J. Phys. Chem.* **1993**, *97*, 9730−9735.
(36) Clarke, T. A.; Mason, R.; Tescari, M. Auger Spectroscopy and Low-Energy Electron Diffraction Studies of Chemisorption of Unsaturated Molecules by (100) Surface of Platinum. *Proc. R. Soc. Lond. A.* **1972**, *331*, 321−333.
(37) Haas, T. W.; Grant, J. T.; Dooley, G. J. Chemical Effects in Auger Electron Spectroscopy. *J. Appl. Phys.* **1972**, *43*, 1853−1860.
(38) Mundschau, M.; Vanselow, R. Growth and Stability of Carbon Islands on Platinum Surfaces. *Surf. Sci.* **1985**, *160*, 23−36.
(39) Enachescu, M.; Schleef, D.; Ogletree, D. F.; Salmeron, M. Integration of Point-Contact Microscopy and Atomic-Force Microscopy: Application to Characterization of Graphite/Pt(111). *Phys. Rev. B* **1999**, *60*, 16913−16919.
(40) Ueta, H.; Saida, M.; Nakai, C.; Yamada, Y.; Sasaki, M.; Yamamoto, S. Highly Oriented Monolayer Graphite Formation on Pt(111) by a Supersonic Methane Beam. *Surf. Sci.* **2004**, *560*, 183−190.
(41) Lang, B. A LEED Study of Deposition of Carbon on Platinum Crystal Surfaces. *Surf. Sci.* **1975**, *53*, 317−329.
(42) Gao, M.; Pan, Y.; Zhang, C.; Hu, H.; Yang, R.; Lu, H.; Cai, J.; Du, S.; Liu, F.; Gao, H.-J. Tunable Interfacial Properties of Epitaxial Graphene on Metal Substrates. *Appl. Phys. Lett.* **2010**, *96*, 053109.
(43) Gao, M.; Pan, Y.; Huang, L.; Hu, H.; Zhang, L. Z.; Guo, H. M.; Du, S. X.; Gao, H.-J. Epitaxial Growth and Structural Property of Graphene on Pt(111). *Appl. Phys. Lett.* **2011**, *98*, 033101.
(44) Gunasooriya, G. T. K. K.; Saeys, M. CO Adsorption on Pt(111): From Isolated Molecules to Ordered High-Coverage Structures. *ACS Catal.* **2018**, *8*, 10225−10233.
(45) Land, T. A.; Michely, T.; Behm, R. J.; Hemminger, J. C.; Comsa, G. STM Investigation of Single Layer Graphite Structures Produced on Pt(111) by Hydrocarbon Decomposition. *Surf. Sci.* **1992**, *264*, 261−270.
(46) Janthon, P.; Viñes, F.; Sirijaraensre, J.; Limtrakul, J.; Illas, F. Carbon Dissolution and Segregation in Platinum. *Catal. Sci. Technol.* **2017**, *7*, 807−816.
(47) Sasaki, M.; Yamada, Y.; Ogiwara, Y.; Yagyu, S.; Yamamoto, S. Moiré Contrast in the Local Tunneling Barrier Height Images of Monolayer Graphite on Pt(111). *Phys. Rev. B* **2000**, *61*, 15653−15656.
(48) Sutter, P.; Sadowski, J. T.; Sutter, E. Graphene on Pt(111): Growth and Substrate Interaction. *Phys. Rev. B* **2009**, *80*, 245411.
(49) Merino, P.; Švec, M.; Pinardi, A. L.; Otero, G.; Martín-Gago, J. A. Strain-Driven Moiré Superstructures of Epitaxial Graphene on Transition Metal Surfaces. *ACS Nano* **2011**, *5*, 5627−5634.
(50) Liang, Z.; Khosravian, H.; Uhl, A.; Meyer, R. J.; Trenary, M. Graphene Domain Boundaries on Pt(111) as Nucleation Sites for Pt Nanocluster Formation. *Surf. Sci.* **2012**, *606*, 1643−1648.
(51) Zi-Pu, H.; Ogletree, D. F.; Van Hove, M. A.; Somorjai, G. A. LEED Theory for Incommensurate Overlayers: Application to Graphite on Pt(111). *Surf. Sci.* **1987**, *180*, 433−459.
(52) Norton, P. R.; Davies, J. A.; Jackman, T. E. Absolute Coverages of CO and O on Pt(111); Comparison of Saturation CO Coverages on Pt(100), (110) and (111) Surfaces. *Surf. Sci.* **1982**, *122*, L593−L600.
(53) Piqué, O.; Koleva, I. Z.; Viñes, F.; Aleksandrov, H. A.; Vayssilov, G. N.; Illas, F. Subsurface Carbon: A General Feature of Noble Metals. *Angew. Chem., Int. Ed.* **2019**, *58*, 1744−1748.
(54) Wrobel, R. J.; Becker, S.; Weiss, H. Influence of Subsurface Oxygen in the Catalytic CO Oxidation on Pd(111). *J. Phys. Chem. C* **2015**, *119*, 5386−5394.

https://dx.doi.org/10.1021/acs.jpcc.0c00160
J. Phys. Chem. C 2020, 124, 6716−6724